Inorganic Chemistry

pubs.acs.org/IC Article

Isolation of a Side-On V(III)-(η^2-O_2) through the Intermediacy of a Low-Valent V(II) in a Metal–Organic Framework

Julius J. Oppenheim, Sujay Bagi, Tianyang Chen, Chenyue Sun, Luming Yang, Peter Müller, Yuriy Román-Leshkov, and Mircea Dincă*

Cite This: *Inorg. Chem.* 2021, 60, 18205–18210 Read Online

ACCESS | Metrics & More | Article Recommendations | Supporting Information

ABSTRACT: We report the isolation of vanadium(II) in a metal–organic framework (MOF) by the reaction of the chloride-capped secondary building unit in the all-vanadium(III) V-MIL-101 (**1**) with 1,4-bis(trimethylsilyl)-2,3,5,6-tetramethyl-1,4-dihydropyrazine. The reduced material, **2**, has a secondary building unit with the formal composition [$V^{II}V_2^{III}$], with each metal ion presenting one open coordination site. Subsequent reaction with O_2 yields a side-on η^2 vanadium-superoxo species, **3**. The MOF featuring V(III)-superoxo moieties exhibits a mild enhancement in the isosteric enthalpy of adsorption for methane compared to the parent V-MIL-101. We present this synthetic methodology as a potentially broad way to access low-valent open metal sites within MOFs without causing a loss of crystallinity or porosity. The low-valent sites can serve as isolable intermediates to access species otherwise inaccessible by direct synthesis.

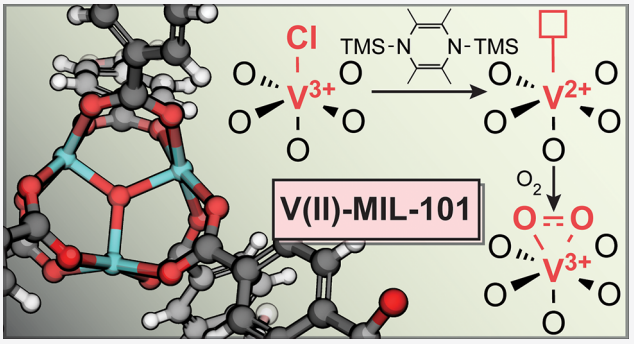

INTRODUCTION

Open metal sites (OMS) within metal–organic frameworks (MOFs) are useful moieties for gas separation, storage, and catalysis due to their direct and chemically specific interactions between the metal and gaseous adsorbates.[1] MOFs with OMS attract attention due to strong host–guest interactions, tunability in the ligand field environment, suppression of bimolecular decomposition pathways, and a wide variety of postfunctionalization.[2,3] Upon the reduction of an OMS, the interaction strength with gaseous adsorbates may increase, permitting difficult gas separations (through strong π-back-bonding interactions) and a broader range of reactivity.[4] The reduction of metal ions within the secondary building units (SBUs) may also afford different types of postfunctionalization (for example, the grafting of anionic ligands). Despite the benefits, synthetic routes for low-valent OMS frameworks have been limited.

Existing routes to generate low-valent OMS frameworks include (1) direct solvothermal reaction using reduced metals,[5,6] (2) postsynthetic metal exchange or metalation,[7−9] and (3) thermal autoreduction.[10,11] Although direct solvothermal synthesis is the most straightforward approach, complications arise because highly reducing metals typically sit negative of the hydrogen evolution potential and thus are incompatible with protic linkers.[12] Hydrogen evolution can be avoided by using the linkers' conjugate base, but aprotic conditions often afford less crystalline products. Postsynthetic metal exchange and metalation do not possess these aforementioned issues but are often limited by an unpredictable extent of exchange and general lack of suitable metal precursors for low-valent metals.[13] Meanwhile, thermal autoreduction reactions are not feasible for every framework due to low-temperature decomposition and amorphization pathways. Likewise, the nature of the reduction is not always obvious because either ligand radical ejection or decarboxylation may occur.[2,14]

Here, we propose postsynthetic chemical reduction as a viable approach. The use of mild salt-free reductants, such as chlorine radical abstractor 1,4-bis(trimethylsilyl)-2,3,5,6-tetramethyl-1,4-dihydropyrazine (Mashima's reagent, $(TMS)_2$pyr), circumvents MOF decomposition through metal-linker bond cleavage and does not cause pore clogging, as salt byproducts of other reducing agents would be expected to.[15,16] Despite its utility in the generation of highly reduced surface sites and the well-defined reduction of molecular organometallic species, Mashima's reagent has seen limited use thus far with MOFs, with the only previous example in the isolation of a Nb(IV) species.[17−21] Here, we demonstrate a wider utility for Mashima's reagent and report the synthesis of V(II)-MIL-

Received: September 13, 2021
Published: November 23, 2021

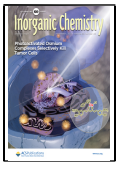

https://doi.org/10.1021/acs.inorgchem.1c02850
Inorg. Chem. 2021, 60, 18205–18210

101, which contains mixed-valent [$V^{II}V_2^{III}$] SBUs, generated by the quantitative reduction of V-MIL-101 (**1**). MIL-101 was chosen as the target system due to the presence of terminal inner-sphere chloride anions, large pores (~30 Å) that can accommodate the bulky reductant, and a convenient continuous flow synthesis that provides higher yields, purity, and shorter reaction times. Notably, V(II)-MIL-101 has not been previously synthesized directly, likely due to the requirement for oxidizing conditions to fill the μ_3-oxo site as well as the tendency for V(II) to facilitate hydrogen evolution.[22] V(II)-MIL-101 serves as a rare example of a vanadium(II) OMS framework.[5,7,8] With the V(II) OMS in hand, we demonstrate the postsynthetic functionalization of **2** with O_2, which yields a side-on metal-superoxo, **3**, that is examined in the context of gas sorption. We further examine analogous processes in a molecular analog, ($V^{II}V_2^{III}$)(μ_3-O)(O_2CPh)$_6$ (**4**).

RESULTS AND DISCUSSION

Synthesis of Frameworks and Molecular Clusters. The MOF V-MIL-101 (**1**) was synthesized using a continuous-flow reactor for the first time.[23−25] The flow reactor (Figure S1) operates in a biphasic liquid−liquid slug flow regime where silicone oil is used as an immiscible continuous phase, which preferentially wets the PTFE reactor tubing and encapsulates the slugs (μL droplets) of the dispersed phase containing the MOF precursors. As the precursor slugs traverse the heated reaction zone, crystallization reactions give rise to viable nucleation sites that emerge from short-range crystalline order, proceeding to grain growth and culminating in MOF crystals. Unlike the traditional batch synthesis, this method enables a higher sample purity, a significantly shorter reaction time (which decreases from 3 days to 1 h), and a higher yield (increases from 28 to 36%) while maintaining its crystallinity and porosity (Figures S2 and S3). This achievement in product intensification is notable because it enables the accelerated manufacturing of V-MIL-101 for further study and is likely to be of use for other systems.

Unlike batch solvothermal syntheses, which are always biphasic with an atmosphere of gas above the reaction mixture, continuous flow syntheses have no gas-phase component. From a mechanistic standpoint, we find that **1** can be synthesized only in high yields and crystallinity when the reaction mixture is initially aerated, whereas little to no material can be recovered upon the addition of any quantity of water. This finding directly implicates dioxygen as the contributor to the μ_3-oxo within the V_3O SBU.

Chlorine radical abstraction and the production of **2** were achieved by the reaction of **1** with $(TMS)_2$pyr in THF at room temperature over the course of 2 days (Figure 1b).[19] Upon reduction, the color of **1** transitions from green to blue-purple (Figure S6). ^{29}Si NMR spectroscopy of the reaction mother liquor indicates the consumption of $(TMS)_2$pyr and the formation of hexamethyldisiloxane, a downstream hydrolysis product of chlorotrimethylsilane (Figure S5). The resultant framework, **2**, is extremely air-sensitive, with trace dioxygen causing irreversible oxidation to a green material, **3**. This irreversible reactivity upon exposure to dioxygen is similar to that observed for MOFs containing Fe(II).[26−28] Compound **3** can be synthesized spontaneously by the exposure of **2** to pure O_2 or to air at room temperature.

Spectroscopic Characterization. Ultraviolet−visible−near-infrared (UV−vis−NIR) and X-ray photoelectron spectroscopies (XPS) provide further support in the assignment of the vanadium oxidation state. The UV−vis−NIR spectrum of **3** matches well with that for **1**, suggesting that the valence of the two systems is similar, namely formally V(III) (Figure S10). The spectrum for **2** reveals additional bands at around 20 000 cm^{-1}. Although we cannot unequivocally assign this band to either d−d excitations or intervalence charge transfer (octahedrally coordinated weak field V(II) ions may have $^4A_{2g} \rightarrow {}^4T_{1g}(^4F)$ absorption bands in this region),[29] the mere appearance of this unique band, which is absent in **1** and **3**, evinces a distinct valency in **2**. X-ray photoelectron spectroscopy of **3** reveals a quantitative depletion of chlorine from the framework (Figures S12 and S13). Given that chloride provides the charge balance for **1** and no chlorine should be eliminated upon exposure of **2** to O_2, we can infer that every SBU in **2** is in the reduced oxidation state.

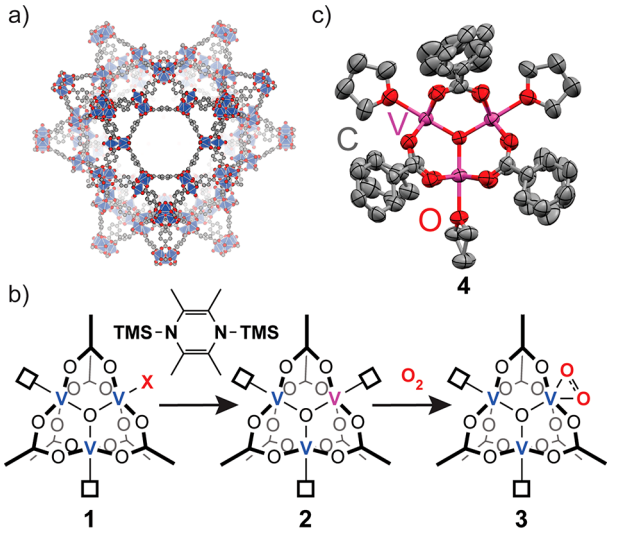

Figure 1. (a) Section of **1** with **mtn-e-a** topology. (b) Synthetic scheme for the isolation of **2** and **3**. (c) Crystal structure of **4**, the molecular analogue of **2** (ORTEP plot with thermal ellipsoids at the 50% probability level; hydrogen atoms and disordered fragments are omitted for clarity).

To provide further evidence for the abstraction of the chlorine radical as opposed to alternative reactivities, we synthesized and crystallized the molecular cluster, ($V^{II}V_2^{III}$)-(μ_3-O)(O_2CPh)$_6$ (**4**), corresponding to the truncation of the SBU in **2**. The precursor to cluster **4** is synthesized under conditions mimicking those for **1**, with benzoic acid as a monotopic replacement for terephthalic acid. Upon reaction of this precursor with stoichiometric equivalents of $(TMS)_2$pyr, a distinct color change from green to purple occurs, similar to the transition observed from **1** to **2**. The UV−vis−NIR spectrum of **4** reveals the appearance of a broad peak ranging from 13 000 to 23 000 cm^{-1} (Figure S11), whose broadness and intensity resemble those commonly observed for intervalence charge-transfer features. X-ray diffraction of a single crystal of **4** grown from THF/pentane (Figure 1c) reveals a formal ($V^{II}V_2^{III}$)(μ_3-O)(O_2CPh)$_6$ cluster capped by three solvent molecules. Framework **2** likely adopts a formal oxidation state combination similar to that for **4**.

Whereas the reaction of 1 equiv of $(TMS)_2$pyr with the molecular analogue of **1** yields **4**, treatment of the parent cluster with excess $(TMS)_2$pyr leads to decomposition and undefined products. Indeed, trigonal trinuclear vanadium

https://doi.org/10.1021/acs.inorgchem.1c02850
Inorg. Chem. 2021, 60, 18205−18210

clusters are known to eliminate carboxylate linkers via silyl ester formation, which can be succeeded by either cluster oligomerization to form polyoxovanadate clusters or by chloride migration to the bridging sites.[30,31] However, the treatment of MOF **1** with excess $(TMS)_2$pyr does not lead to polyoxovanadate formation, halting at chlorine radical abstraction. This notable difference in reactivity likely arises as a direct consequence of site isolation and the rigidity of the framework, which allow access of the reductant to chloride but not to the carboxylates.

Structural Characterization of the Frameworks and Molecular Cluster. Pawley refinement of powder X-ray diffractograms (PXRD) collected in transmission mode provides information about the purity of the compounds and the structural changes brought about by postsynthetic modifications. PXRD of **1** matches well with the predicted structure for V-MIL-101.[32] PXRD of **2** reveals that upon reduction there is a 1.6% increase in the cell parameter compared to that of **1** (90.15(2) Å for **2** compared to 88.77(3) Å for **1**[32]), commensurate with the expectation for bond lengthening upon reduction (Figure 2). PXRD of **3** reveals a

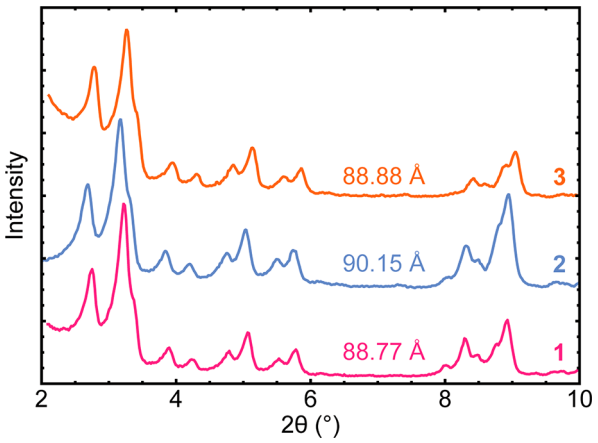

Figure 2. Powder X-ray diffractograms of **1**, **2**, and **3** and their Pawley refined unit cell parameters (space group $Fd\bar{3}m$ with $a = b = c$).

contraction of cell parameters back to those of **1** (88.88(3) Å for **3**). Notably, there are no changes in the broadness of diffraction peaks or the appearance of additional peaks, indicating a retention of crystallinity throughout the transformations. Transmission electron microscopy of **1** reveals particle sizes of ∼100 nm, in agreement with the broad peaks observed by PXRD (Figure S4).

Powder X-ray diffractograms reveal a slight quantity of VO_2 impurities in samples of **1** prepared by batch synthesis. These impurities are absent when the MOF is prepared by continuous flow synthesis (Figure S2). The oxide impurities are detrimental to the activation of **2** due to the behavior of vanadium oxides to reductively eliminate dioxygen under ultrahigh vacuum and elevated temperatures, which can subsequently react with the framework to form **3**.[33]

A comparison of the molecular cluster to the frameworks was used as a proxy to determine the structural information about **2**. The reduced molecular cluster, **4**, crystallizes in the monoclinic $C2/c$ space group with two independent V_3O units in the asymmetric unit. Because of the large disorder seen with crystals of **4**, there is a large distribution in the V−O bond lengths, which average 2.036(4) and 1.916(4) Å for V−O (O_2CPh) and V−O (μ_3-O) (Table S4). These values are similar to those for the only other reported $[V^{II}V_2^{III}]$ cluster (capped with trifluoroacetate ligands), which display lengths of 2.040(7) and 1.935(6) Å.[34] The V−O (O_2CPh) bond length is 1.4% longer than the average V−O (O_2CEt) bond length of the previously reported all-V(III) cluster at 2.008(4) Å.[35] Conversely, the average V−O (μ_3-O) bond length is slightly contracted compared to the oxidized cluster at 1.928(4) Å. These results suggest that the 1.6% increase in the unit cell size for **2** relative to **1** is likely due to the elongation of the V−O (O_2CPh) bonds. This may correspond to the occupation of d_{xy} metal−ligand antibonding orbitals (defining the z-axis along the V−O (μ_3-O) bond) or may be due to changes in the Coulombic attraction between vanadium and the carboxylate. It is not possible to determine whether there is valence trapping of the $[V^{II}V_2^{III}]$ state because no distortions from 3-fold symmetry can be observed. The lack of distortion may result from either valence delocalization or crystallographic disorder.

Vibrational Spectroscopy. In situ diffuse reflectance infrared Fourier transform (DRIFT) and Raman spectroscopies reveal that O_2 bound to **3** is coordinated as a side-on superoxo. Upon dosing $^{16}O_2$ or $^{18}O_2$, the carboxylate symmetric and antisymmetric stretching bands (near 1400 and 1600 cm^{-1}) shift to higher energies (Figures S15−S17), symptomatic of an oxidative event at the metal centers.

A noticeable absorption band at 1013 cm^{-1} grows in upon dosing **2** with $^{16}O_2$, which shifts to 968 cm^{-1} upon dosing **2** with $^{18}O_2$, suggesting that these stretching modes involve oxygen (Figure 3). These bands persist even after the storage

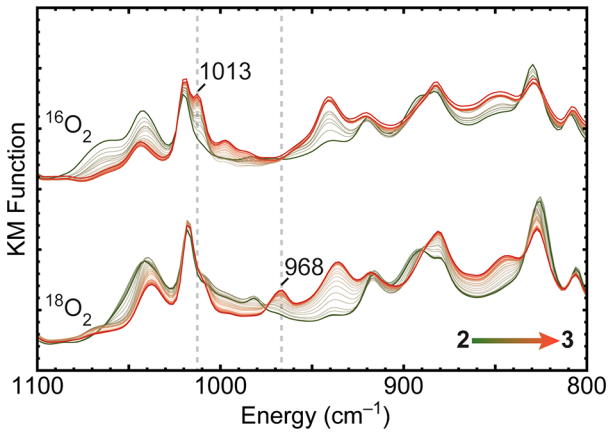

Figure 3. Diffuse reflectance infrared Fourier transform (DRIFT) spectra upon dosing **2** with $^{18}O_2$ and $^{16}O_2$, green to red, respectively.

of **3** in air for 1 day (Figure S16), suggesting that further reactivity with O_2 and water is slow. Specifically, oxygen-involving vibrational modes in this energy range are indicative of O−O stretching modes, the energy of which can be correlated to the bond order and thus an assignment of whether it has superoxo or peroxo character. Dioxygen species are typically classified as end-on η^1 superoxo species (between 1050 and 1200 cm^{-1}) or side-on η^2 peroxo species (between 800 and 930 cm^{-1}).[36,37] Bound dioxygen species with stretching frequencies that lie between these two regimes often fall into the less common category of side-on η^2 superoxo species. Such species are rarer than either end-on superoxo or side-on peroxo species. The isotopic shift of 45 cm^{-1} is slightly less than that predicted by a harmonic oscillator approximation

https://doi.org/10.1021/acs.inorgchem.1c02850
Inorg. Chem. 2021, 60, 18205−18210

(58 cm^{-1}), suggesting that the vibrational mode is not that of a pure O−O stretch. The binding mode of dioxygen to **3** is most similar to that of a side-on superoxo species, which has $\nu(^{16}O-^{16}O)$ at 1027 cm^{-1} and $\nu(^{18}O-^{18}O)$ at 969 cm^{-1}, as observed in a crystallographically characterized Cr(III) complex.[38] The molecular cluster analogue of **3** could not be isolated to corroborate the assignment of a side-on superoxo, possibly due to bimolecular O_2 activation. This discrepancy reflects another benefit of using MOFs as a platform for heterogeneous catalysis because site isolation allows for the isolation of reactive species not easily stabilized by molecular complexes.

Gas Sorption. Gas sorption measurements were conducted to study changes in the surface areas of **1** and **3**. Upon the transformation of **1** to **3**, the BET surface area (measured at 77 K with N_2) decreases slightly from 2075 to 1884 m^2/g (Figure S9). The characteristic stepwise isotherm shape of MIL-101 is preserved, revealing that the pore size and shape of **3** are comparable to those of **1**.

Variable-temperature adsorption isotherms at 15 and 25 °C for CO_2, CH_4, ethylene, and ethane within **1** and **3** were used to determine the strength of the interaction of the framework with each gas. Upon conversion of **1** to **3**, the uptake capacity (measured at 700 Torr at 25 °C) for CO_2 decreased from 34.3 to 25.3 cm^3/g, decreased for C_2H_4 from 29.0 to 23.6 cm^3/g, and decreased for C_2H_6 from 30.3 to 15.0 cm^3/g. Meanwhile, the uptake capacity increased for CH_4 from 10.5 to 13.0 cm^3/g. There is no discernible trend in the changes in uptake capacity. Isosteric enthalpies of adsorption were calculated by fitting the data with a dual-site Langmuir model (Figures 4 and S18, Tables S2 and S3). There is a slight increase in the isosteric enthalpy of adsorption in the low-coverage limit for all gases except ethylene (Table S2). Unlike similar dioxygen-bound functional sites within peroxo-Fe-MOF-74 that confer selectivity for alkanes over alkenes,[3] the dioxygen sites in **3** provide no strong preferential uptake for either ethane or ethylene. These results may suggest that these four sorbates primarily coordinate to the coordinatively unsaturated vanadium sites (rather than the chloride or dioxygen bound sites) at low coverage, and as such, there are no significant changes upon anion exchange. Sorption experiments of **2** were all unsuccessful due to partial oxidation with trace dioxygen.

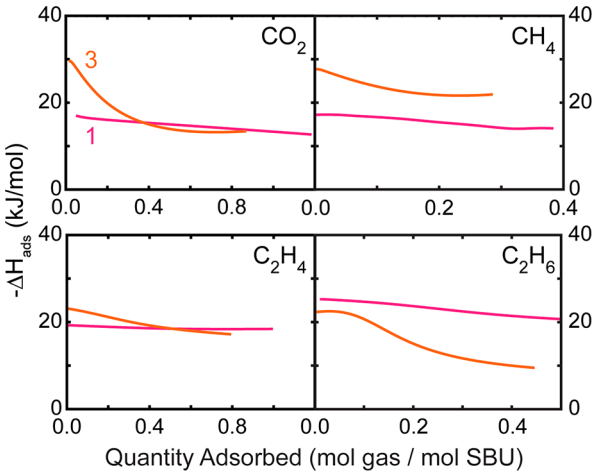

Figure 4. Isosteric enthalpies of adsorption for carbon dioxide, methane, ethylene, and ethane in **1** and **3**.

CONCLUSIONS

Here, we have demonstrated the well-defined sequential reactivity of V-MIL-101 by initial reduction with a salt-free chlorine radical abstracting reagent, $(TMS)_2$pyr, followed by oxidation with O_2 to form a side-on vanadium-superoxo. Continuous flow synthesis demonstrates the preparation of V-MIL-101 with improved reaction times, yields, and phase purity. The reduced framework, **2**, is a rare example of a vanadium(II)-bearing MOF, and the methodology for its synthesis may be transferrable to other systems. The reactivity of **2** with O_2 to form superoxo-bearing **3** is quite surprising because dioxygen-bound vanadium complexes are typically difficult to isolate in the absence of bulky steric protection to prevent bimolecular reactivity.[39] This difference demonstrates the benefits of site isolation within the heterogeneous MOF support. We anticipate that this methodology of postsynthetic reduction will enable the access of other low-valent, coordinatively unsaturated metal species within MOFs.

ASSOCIATED CONTENT

Supporting Information

The Supporting Information is available free of charge at https://pubs.acs.org/doi/10.1021/acs.inorgchem.1c02850.

Synthetic methods, Pawley refinements, gas sorption isotherms and isosteric enthalpy of adsorption calculations, NMR spectra, UV−visible−near IR spectra, X-ray photoelectron spectra, thermogravimetric analyses, Raman spectra, and crystallographic information (PDF)

Accession Codes

CCDC 2109241 contains the supplementary crystallographic data for this paper. These data can be obtained free of charge via www.ccdc.cam.ac.uk/data_request/cif, or by emailing data_request@ccdc.cam.ac.uk, or by contacting The Cambridge Crystallographic Data Centre, 12 Union Road, Cambridge CB2 1EZ, UK; fax: +44 1223 336033.

AUTHOR INFORMATION

Corresponding Author

Mircea Dincă − *Department of Chemistry, Massachusetts Institute of Technology, Cambridge, Massachusetts 02139, United States;* orcid.org/0000-0002-1262-1264; Email: mdinca@mit.edu

Authors

Julius J. Oppenheim − *Department of Chemistry, Massachusetts Institute of Technology, Cambridge, Massachusetts 02139, United States*

Sujay Bagi − *Department of Chemical Engineering and Department of Mechanical Engineering, Massachusetts Institute of Technology, Cambridge, Massachusetts 02139, United States*

Tianyang Chen − *Department of Chemistry, Massachusetts Institute of Technology, Cambridge, Massachusetts 02139, United States;* orcid.org/0000-0003-3142-8176

Chenyue Sun − *Department of Chemistry, Massachusetts Institute of Technology, Cambridge, Massachusetts 02139, United States*

Luming Yang − *Department of Chemistry, Massachusetts Institute of Technology, Cambridge, Massachusetts 02139, United States*

Peter Müller − *Department of Chemistry, Massachusetts Institute of Technology, Cambridge, Massachusetts 02139, United States;* orcid.org/0000-0001-6530-3852

Yuriy Román-Leshkov − *Department of Chemical Engineering, Massachusetts Institute of Technology, Cambridge, Massachusetts 02139, United States;* orcid.org/0000-0002-0025-4233

Complete contact information is available at: https://pubs.acs.org/10.1021/acs.inorgchem.1c02850

Funding

Work in the Dincă laboratory was supported by the National Science Foundation (Waterman award to M.D.; DMR-1645232). Work in the Roman laboratory was supported by the U.S. Department of Energy, Office of Basic Energy Sciences under award DE-SC0016214 for support. This work made use of an X-ray diffractometer purchased with funds from the National Science Foundation (CHE-0946721) and of Shared Experimental Facilities supported in part by the MRSEC Program of the National Science Foundation (DMR-1419807).

Notes

The authors declare no competing financial interest.

■ ACKNOWLEDGMENTS

We thank Professor Zachary Smith and Wan-Ni Wu for useful discussions.

■ REFERENCES

(1) Kökçam-Demir, Ü.; Goldman, A.; Esrafili, L.; Gharib, M.; Morsali, A.; Weingart, O.; Janiak, C. Coordinatively Unsaturated Metal Sites (Open Metal Sites) in Metal−Organic Frameworks: Design and Applications. *Chem. Soc. Rev.* **2020**, *49* (9), 2751−2798.

(2) Wang, W.; Sharapa, D. I.; Chandresh, A.; Nefedov, A.; Heißler, S.; Heinke, L.; Studt, F.; Wang, Y.; Wöll, C. Interplay of Electronic and Steric Effects to Yield Low-Temperature CO Oxidation at Metal Single Sites in Defect-Engineered HKUST-1. *Angew. Chem., Int. Ed.* **2020**, *59* (26), 10514−10518.

(3) Li, L.; Lin, R.-B.; Krishna, R.; Li, H.; Xiang, S.; Wu, H.; Li, J.; Zhou, W.; Chen, B. Ethane/Ethylene Separation in a Metal-Organic Framework with Iron-Peroxo Sites. *Science* **2018**, *362* (6413), 443−446.

(4) Lee, K.; Isley, W. C., III; Dzubak, A. L.; Verma, P.; Stoneburner, S. J.; Lin, L.-C.; Howe, J. D.; Bloch, E. D.; Reed, D. A.; Hudson, M. R.; et al. Design of a Metal−Organic Framework with Enhanced Back Bonding for Separation of N2 and CH4. *J. Am. Chem. Soc.* **2014**, *136* (2), 698−704.

(5) Jaramillo, D. E.; Reed, D. A.; Jiang, H. Z.; Oktawiec, J.; Mara, M. W.; Forse, A. C.; Lussier, D. J.; Murphy, R. A.; Cunningham, M.; Colombo, V.; et al. Selective Nitrogen Adsorption via Backbonding in a Metal−Organic Framework with Exposed Vanadium Sites. *Nat. Mater.* **2020**, *19* (5), 517−521.

(6) Mason, J. A.; Darago, L. E.; Lukens, W. W., Jr; Long, J. R. Synthesis and O2 Reactivity of a Titanium (III) Metal−Organic Framework. *Inorg. Chem.* **2015**, *54* (20), 10096−10104.

(7) Brozek, C. K.; Dincă, M. Ti3+-, V2+/3+-, Cr2+/3+-, Mn2+-, and Fe2+-Substituted MOF-5 and Redox Reactivity in Cr- and Fe-MOF-5. *J. Am. Chem. Soc.* **2013**, *135* (34), 12886−12891.

(8) Comito, R. J.; Wu, Z.; Zhang, G.; Lawrence, J. A.; Korzyński, M. D.; Kehl, J. A.; Miller, J. T.; Dincă, M. Stabilized Vanadium Catalyst for Olefin Polymerization by Site Isolation in a Metal−Organic Framework. *Angew. Chem., Int. Ed.* **2018**, *57* (27), 8135−8139.

(9) Kaye, S. S.; Long, J. R. Matrix Isolation Chemistry in a Porous Metal−Organic Framework: Photochemical Substitutions of N2 and H2 in Zn4O[(H6−1,4-Benzenedicarboxylate)Cr(CO)3]3. *J. Am. Chem. Soc.* **2008**, *130* (3), 806−807.

(10) Hall, J. N.; Bollini, P. Enabling Access to Reduced Open-Metal Sites in Metal-Organic Framework Materials through Choice of Anion Identity: The Case of MIL-100(Cr). *ACS Materials Lett.* **2020**, *2* (7), 838−844.

(11) Vimont, A.; Goupil, J.-M.; Lavalley, J.-C.; Daturi, M.; Surblé, S.; Serre, C.; Millange, F.; Férey, G.; Audebrand, N. Investigation of Acid Sites in a Zeotypic Giant Pores Chromium(III) Carboxylate. *J. Am. Chem. Soc.* **2006**, *128* (10), 3218−3227.

(12) Kramer, M.; Schwarz, U.; Kaskel, S. Synthesis and Properties of the Metal-Organic Framework Mo3(BTC)2 (TUDMOF-1). *J. Mater. Chem.* **2006**, *16* (23), 2245−2248.

(13) Yin, Z.; Wan, S.; Yang, J.; Kurmoo, M.; Zeng, M.-H. Recent Advances in Post-Synthetic Modification of Metal−Organic Frameworks: New Types and Tandem Reactions. *Coord. Chem. Rev.* **2019**, *378*, 500−512.

(14) Yoon, J. W.; Seo, Y.-K.; Hwang, Y. K.; Chang, J.-S.; Leclerc, H.; Wuttke, S.; Bazin, P.; Vimont, A.; Daturi, M.; Bloch, E.; Llewellyn, P. L.; Serre, C.; Horcajada, P.; Grenèche, J.-M.; Rodrigues, A. E.; Férey, G. Controlled Reducibility of a Metal−Organic Framework with Coordinatively Unsaturated Sites for Preferential Gas Sorption. *Angew. Chem., Int. Ed.* **2010**, *49* (34), 5949−5952.

(15) Biggins, N.; Ziebel, M. E.; Gonzalez, M. I.; Long, J. R. Crystallographic Characterization of the Metal−Organic Framework Fe2(Bdp)3 upon Reductive Cation Insertion. *Chem. Sci.* **2020**, *11* (34), 9173−9180.

(16) Prabhakaran, P. K.; Deschamps, J. Doping Activated Carbon Incorporated Composite MIL-101 Using Lithium: Impact on Hydrogen Uptake. *J. Mater. Chem. A* **2015**, *3* (13), 7014−7021.

(17) Korzyński, M. D.; Braglia, L.; Borfecchia, E.; Lomachenko, K. A.; Baldansuren, A.; Hendon, C. H.; Lamberti, C.; Dincă, M. Quo Vadis Niobium? Divergent Coordination Behavior of Early-Transition Metals towards MOF-5. *Chem. Sci.* **2019**, *10* (23), 5906−5910.

(18) Mougel, V.; Chan, K.-W.; Siddiqi, G.; Kawakita, K.; Nagae, H.; Tsurugi, H.; Mashima, K.; Safonova, O.; Copéret, C. Low Temperature Activation of Supported Metathesis Catalysts by Organosilicon Reducing Agents. *ACS Cent. Sci.* **2016**, *2* (8), 569−576.

(19) Tsurugi, H.; Mashima, K. Salt-Free Reduction of Transition Metal Complexes by Bis (Trimethylsilyl) Cyclohexadiene,-Dihydropyrazine, and-4, 4′-Bipyridinylidene Derivatives. *Acc. Chem. Res.* **2019**, *52* (3), 769−779.

(20) Saito, T.; Nishiyama, H.; Tanahashi, H.; Kawakita, K.; Tsurugi, H.; Mashima, K. 1,4-Bis(Trimethylsilyl)-1,4-Diaza-2,5-Cyclohexadienes as Strong Salt-Free Reductants for Generating Low-Valent Early Transition Metals with Electron-Donating Ligands. *J. Am. Chem. Soc.* **2014**, *136* (13), 5161−5170.

(21) Kawakita, K.; Beaumier, E. P.; Kakiuchi, Y.; Tsurugi, H.; Tonks, I. A.; Mashima, K. Bis(Imido)Vanadium(V)-Catalyzed [2 + 2+1] Coupling of Alkynes and Azobenzenes Giving Multisubstituted Pyrroles. *J. Am. Chem. Soc.* **2019**, *141* (10), 4194−4198.

(22) Povar, I.; Spinu, O.; Zinicovscaia, I.; Pintilie, B.; Ubaldini, S. Revised Pourbaix Diagrams for the Vanadium − Water System. *J. Electrochem. Sci. Eng.* **2019**, *9* (2), 75−84.

(23) Bagi, S.; Wright, A. M.; Oppenheim, J.; Dincă, M.; Román-Leshkov, Y. Accelerated Synthesis of a Ni2Cl2(BTDD) Metal−Organic Framework in a Continuous Flow Reactor for Atmospheric Water Capture. *ACS Sustainable Chem. Eng.* **2021**, *9* (11), 3996−4003.

(24) Bagi, S. D.; Myerson, A. S.; Román-Leshkov, Y. Solvothermal Crystallization Kinetics and Control of Crystal Size Distribution of MOF-808 in a Continuous Flow Reactor. *Cryst. Growth Des.* **2021**, *21*, 6529.

(25) Bagi, S. D.; Yuan, S.; Rojas-Buzo, S.; Shao-Horn, Y.; Roman-Leshkov, Y. A Continuous Flow Chemistry Approach for the Ultrafast and Low-Cost Synthesis of MOF-808. *Green Chem.* **2021**, DOI: 10.1039/D1GC02824C.

(26) Bloch, E. D.; Murray, L. J.; Queen, W. L.; Chavan, S.; Maximoff, S. N.; Bigi, J. P.; Krishna, R.; Peterson, V. K.; Grandjean,

F.; Long, G. J.; Smit, B.; Bordiga, S.; Brown, C. M.; Long, J. R. Selective Binding of O2 over N2 in a Redox−Active Metal−Organic Framework with Open Iron(II) Coordination Sites. *J. Am. Chem. Soc.* **2011**, *133* (37), 14814−14822.
(27) Jaffe, A.; Ziebel, M. E.; Halat, D. M.; Biggins, N.; Murphy, R. A.; Chakarawet, K.; Reimer, J. A.; Long, J. R. Selective, High-Temperature O2 Adsorption in Chemically Reduced, Redox-Active Iron-Pyrazolate Metal−Organic Frameworks. *J. Am. Chem. Soc.* **2020**, *142* (34), 14627−14637.
(28) Reed, D. A.; Xiao, D. J.; Jiang, H. Z.; Chakarawet, K.; Oktawiec, J.; Long, J. R.; Biomimetic, O. Biomimetic O2 Adsorption in an Iron Metal−Organic Framework for Air Separation. *Chem. Sci.* **2020**, *11* (6), 1698−1702.
(29) Jorgensen, C. Ligand Field Spectrum of Vanadium (II) Hexaquo Ions. *Acta Chem. Scand.* **1958**, *12* (7), 1537−1538.
(30) Kazuhiko, S.; Matsumoto, K.; Kazuyuki, M.; Hayato, T.; Hirotaka, O.; Takaya, T. Method for Producing Polynuclear Metal Cluster. JP Patent 2020143003, September 10, 2020.
(31) Yuge, H.; Asahi, S.; Miyamoto, T. K. A New Route for Substitution of the Bridging Acetate on the Oxo-Centered Triruthenium Acetate Cluster. *Dalton Trans.* **2009**, No. 13, 2287−2289.
(32) Biswas, S.; Couck, S.; Grzywa, M.; Denayer, J. F. M.; Volkmer, D.; Voort, P. V. D. Vanadium Analogues of Nonfunctionalized and Amino-Functionalized MOFs with MIL-101 Topology − Synthesis, Characterization, and Gas Sorption Properties. *Eur. J. Inorg. Chem.* **2012**, *2012* (15), 2481−2486.
(33) Wu, Q.-H.; Thissen, A.; Jaegermann, W.; Liu, M. Photoelectron Spectroscopy Study of Oxygen Vacancy on Vanadium Oxides Surface. *Appl. Surf. Sci.* **2004**, *236* (1−4), 473−478.
(34) Cotton, F. A.; Lewis, G. E.; Mott, G. N. New Trinuclear, Oxo-Centered, Basic Carboxylate Compounds of Transition Metals. 3. Syntheses and x-Ray Studies of the Trivanadium(III,III,III) and Trivanadium(II,III,III) Compounds [V3(.Mu.3-O)(CH3CO2)6-(CH3COOH)2(THF)]+[VCl4(CH3COOH)2]- and V3(.Mu.3-O)-(CF3CO2)6(THF)3 with "Classical" Triangular Structures. *Inorg. Chem.* **1982**, *21* (9), 3316−3321.
(35) Castro, S. L.; Streib, W. E.; Sun, J.-S.; Christou, G. Structural, Spectroscopic, and Magnetochemical Characterization of the Trinuclear Vanadium (III) Carboxylates [V3O (O2CR) 6L3](ClO4)-(R= Various Groups; L= Pyridine, 4-Picoline, 3, 5-Lutidine). *Inorg. Chem.* **1996**, *35* (15), 4462−4468.
(36) Cramer, C. J.; Tolman, W. B.; Theopold, K. H.; Rheingold, A. L. Variable Character of O—O and M—O Bonding in Side-on (H2) 1:1 Metal Complexes of O2. *Proc. Natl. Acad. Sci. U. S. A.* **2003**, *100* (7), 3635−3640.
(37) Egan, J. W.; Haggerty, B. S.; Rheingold, A. L.; Sendlinger, S. C.; Theopold, K. H. Crystal Structure of a Side-on Superoxo Complex of Cobalt and Hydrogen Abstraction by a Reactive Terminal Oxo Ligand. *J. Am. Chem. Soc.* **1990**, *112* (6), 2445−2446.
(38) Qin, K.; Incarvito, C. D.; Rheingold, A. L.; Theopold, K. H. A Structurally Characterized Chromium(III) Superoxide Complex Features "Side-on" Bonding. *Angew. Chem., Int. Ed.* **2002**, *41* (13), 2333−2335.
(39) Meyer, R. L.; Miró, P.; Brennessel, W. W.; Matson, E. M. O2 Activation with a Sterically Encumbered, Oxygen-Deficient Poly-oxovanadate-Alkoxide Cluster. *Inorg. Chem.* **2021**, *60*, 13833.

https://doi.org/10.1021/acs.inorgchem.1c02850
Inorg. Chem. 2021, 60, 18205−18210